Source breakup dynamics in Au+Au Collisions at $\sqrt{s_{NN}}$=200 GeV via three-dimensional two-pion source imaging

S. Afanasiev,[17] C. Aidala,[7] N.N. Ajitanand,[43] Y. Akiba,[37, 38] J. Alexander,[43] A. Al-Jamel,[33] K. Aoki,[23, 37] L. Aphecetche,[45] R. Armendariz,[33] S.H. Aronson,[3] R. Averbeck,[44] T.C. Awes,[34] B. Azmoun,[3] V. Babintsev,[14] A. Baldisseri,[8] K.N. Barish,[4] P.D. Barnes,[26] B. Bassalleck,[32] S. Bathe,[4] S. Batsouli,[7] V. Baublis,[36] F. Bauer,[4] A. Bazilevsky,[3] S. Belikov,[3, 16, *] R. Bennett,[44] Y. Berdnikov,[40] M.T. Bjorndal,[7] J.G. Boissevain,[26] H. Borel,[8] K. Boyle,[44] M.L. Brooks,[26] D.S. Brown,[33] D. Bucher,[29] H. Buesching,[3] V. Bumazhnov,[14] G. Bunce,[3, 38] J.M. Burward-Hoy,[26] S. Butsyk,[44] S. Campbell,[44] J.-S. Chai,[18] S. Chernichenko,[14] J. Chiba,[19] C.Y. Chi,[7] M. Chiu,[7] I.J. Choi,[52] T. Chujo,[49] P. Chung,[43] V. Cianciolo,[34] C.R. Cleven,[12] Y. Cobigo,[8] B.A. Cole,[7] M.P. Comets,[35] P. Constantin,[16] M. Csanád,[10] T. Csörgő,[20] T. Dahms,[44] K. Das,[11] G. David,[3] H. Delagrange,[45] A. Denisov,[14] D. d'Enterria,[7] A. Deshpande,[38, 44] E.J. Desmond,[3] O. Dietzsch,[41] A. Dion,[44] J.L. Drachenberg,[1] O. Drapier,[24] A. Drees,[44] A.K. Dubey,[51] A. Durum,[14] V. Dzhordzhadze,[46] Y.V. Efremenko,[34] J. Egdemir,[44] A. Enokizono,[13] H. En'yo,[37, 38] B. Espagnon,[35] S. Esumi,[48] D.E. Fields,[32, 38] F. Fleuret,[24] S.L. Fokin,[22] B. Forestier,[27] Z. Fraenkel,[51] J.E. Frantz,[7] A. Franz,[3] A.D. Frawley,[11] Y. Fukao,[23, 37] S.-Y. Fung,[4] S. Gadrat,[27] F. Gastineau,[45] M. Germain,[45] A. Glenn,[46] M. Gonin,[24] J. Gosset,[8] Y. Goto,[37, 38] R. Granier de Cassagnac,[24] N. Grau,[16] S.V. Greene,[49] M. Grosse Perdekamp,[15, 38] T. Gunji,[5] H.-Å. Gustafsson,[28] T. Hachiya,[13, 37] A. Hadj Henni,[45] J.S. Haggerty,[3] M.N. Hagiwara,[1] H. Hamagaki,[5] H. Harada,[13] E.P. Hartouni,[25] K. Haruna,[13] M. Harvey,[3] E. Haslum,[28] K. Hasuko,[37] R. Hayano,[5] M. Heffner,[25] T.K. Hemmick,[44] J.M. Heuser,[37] X. He,[12] H. Hiejima,[15] J.C. Hill,[16] R. Hobbs,[32] M. Holmes,[49] W. Holzmann,[43] K. Homma,[13] B. Hong,[21] T. Horaguchi,[37, 47] M.G. Hur,[18] T. Ichihara,[37, 38] K. Imai,[23, 37] M. Inaba,[48] D. Isenhower,[1] L. Isenhower,[1] M. Ishihara,[37] T. Isobe,[5] M. Issah,[43] A. Isupov,[17] B.V. Jacak,[44, †] J. Jia,[7] J. Jin,[7] O. Jinnouchi,[38] B.M. Johnson,[3] K.S. Joo,[30] D. Jouan,[35] F. Kajihara,[5, 37] S. Kametani,[5, 50] N. Kamihara,[37, 47] M. Kaneta,[38] J.H. Kang,[52] T. Kawagishi,[48] A.V. Kazantsev,[22] S. Kelly,[6] A. Khanzadeev,[36] D.J. Kim,[52] E. Kim,[42] Y.-S. Kim,[18] E. Kinney,[6] A. Kiss,[10] E. Kistenev,[3] A. Kiyomichi,[37] C. Klein-Boesing,[29] L. Kochenda,[36] V. Kochetkov,[14] B. Komkov,[36] M. Konno,[48] D. Kotchetkov,[4] A. Kozlov,[51] P.J. Kroon,[3] G.J. Kunde,[26] N. Kurihara,[5] K. Kurita,[39, 37] M.J. Kweon,[21] Y. Kwon,[52] G.S. Kyle,[33] R. Lacey,[43] J.G. Lajoie,[16] A. Lebedev,[16] Y. Le Bornec,[35] S. Leckey,[44] D.M. Lee,[26] M.K. Lee,[52] M.J. Leitch,[26] M.A.L. Leite,[41] H. Lim,[42] A. Litvinenko,[17] M.X. Liu,[26] X.H. Li,[4] C.F. Maguire,[49] Y.I. Makdisi,[3] A. Malakhov,[17] M.D. Malik,[32] V.I. Manko,[22] H. Masui,[48] F. Matathias,[44] M.C. McCain,[15] P.L. McGaughey,[26] Y. Miake,[48] T.E. Miller,[49] A. Milov,[44] S. Mioduszewski,[3] G.C. Mishra,[12] J.T. Mitchell,[3] D.P. Morrison,[3] J.M. Moss,[26] T.V. Moukhanova,[22] D. Mukhopadhyay,[49] J. Murata,[39, 37] S. Nagamiya,[19] Y. Nagata,[48] J.L. Nagle,[6] M. Naglis,[51] T. Nakamura,[13] J. Newby,[25] M. Nguyen,[44] B.E. Norman,[26] A.S. Nyanin,[22] J. Nystrand,[28] E. O'Brien,[3] C.A. Ogilvie,[16] H. Ohnishi,[37] I.D. Ojha,[49] H. Okada,[23, 37] K. Okada,[38] O.O. Omiwade,[1] A. Oskarsson,[28] I. Otterlund,[28] K. Ozawa,[5] D. Pal,[49] A.P.T. Palounek,[26] V. Pantuev,[44] V. Papavassiliou,[33] J. Park,[42] W.J. Park,[21] S.F. Pate,[33] H. Pei,[16] J.-C. Peng,[15] H. Pereira,[8] V. Peresedov,[17] D.Yu. Peressounko,[22] C. Pinkenburg,[3] R.P. Pisani,[3] M.L. Purschke,[3] A.K. Purwar,[44] H. Qu,[12] J. Rak,[16] I. Ravinovich,[51] K.F. Read,[34, 46] M. Reuter,[44] K. Reygers,[29] V. Riabov,[36] Y. Riabov,[36] G. Roche,[27] A. Romana,[24, *] M. Rosati,[16] S.S.E. Rosendahl,[28] P. Rosnet,[27] P. Rukoyatkin,[17] V.L. Rykov,[37] S.S. Ryu,[52] B. Sahlmueller,[29] N. Saito,[23, 37, 38] T. Sakaguchi,[5, 50] S. Sakai,[48] V. Samsonov,[36] H.D. Sato,[23, 37] S. Sato,[3, 19, 48] S. Sawada,[19] V. Semenov,[14] R. Seto,[4] D. Sharma,[51] T.K. Shea,[3] I. Shein,[14] T.-A. Shibata,[37, 47] K. Shigaki,[13] M. Shimomura,[48] T. Shohjoh,[48] K. Shoji,[23, 37] A. Sickles,[44] C.L. Silva,[41] D. Silvermyr,[34] K.S. Sim,[21] C.P. Singh,[2] V. Singh,[2] S. Skutnik,[16] W.C. Smith,[1] A. Soldatov,[14] R.A. Soltz,[25] W.E. Sondheim,[26] S.P. Sorensen,[46] I.V. Sourikova,[3] F. Staley,[8] P.W. Stankus,[34] E. Stenlund,[28] M. Stepanov,[33] A. Ster,[20] S.P. Stoll,[3] T. Sugitate,[13] C. Suire,[35] J.P. Sullivan,[26] J. Sziklai,[20] T. Tabaru,[38] S. Takagi,[48] E.M. Takagui,[41] A. Taketani,[37, 38] K.H. Tanaka,[19] Y. Tanaka,[31] K. Tanida,[37, 38] M.J. Tannenbaum,[3] A. Taranenko,[43] P. Tarján,[9] T.L. Thomas,[32] M. Togawa,[23, 37] J. Tojo,[37] H. Torii,[37] R.S. Towell,[1] V-N. Tram,[24] I. Tserruya,[51] Y. Tsuchimoto,[13, 37] S.K. Tuli,[2] H. Tydesjö,[28] N. Tyurin,[14] C. Vale,[16] H. Valle,[49] H.W. van Hecke,[26] J. Velkovska,[49] R. Vertesi,[9] A.A. Vinogradov,[22] E. Vznuzdaev,[36] M. Wagner,[23, 37] X.R. Wang,[33] Y. Watanabe,[37, 38] J. Wessels,[29] S.N. White,[3] N. Willis,[35] D. Winter,[7] C.L. Woody,[3] M. Wysocki,[6] W. Xie,[4, 38] A. Yanovich,[14] S. Yokkaichi,[37, 38] G.R. Young,[34] I. Younus,[32] I.E. Yushmanov,[22] W.A. Zajc,[7] O. Zaudtke,[29] C. Zhang,[7] J. Zimányi,[20, *] and L. Zolin[17]

(PHENIX Collaboration)

[1] Abilene Christian University, Abilene, TX 79699, USA

[2]*Department of Physics, Banaras Hindu University, Varanasi 221005, India*
[3]*Brookhaven National Laboratory, Upton, NY 11973-5000, USA*
[4]*University of California - Riverside, Riverside, CA 92521, USA*
[5]*Center for Nuclear Study, Graduate School of Science, University of Tokyo, 7-3-1 Hongo, Bunkyo, Tokyo 113-0033, Japan*
[6]*University of Colorado, Boulder, CO 80309, USA*
[7]*Columbia University, New York, NY 10027 and Nevis Laboratories, Irvington, NY 10533, USA*
[8]*Dapnia, CEA Saclay, F-91191, Gif-sur-Yvette, France*
[9]*Debrecen University, H-4010 Debrecen, Egyetem tér 1, Hungary*
[10]*ELTE, Eötvös Loránd University, H - 1117 Budapest, Pázmány P. s. 1/A, Hungary*
[11]*Florida State University, Tallahassee, FL 32306, USA*
[12]*Georgia State University, Atlanta, GA 30303, USA*
[13]*Hiroshima University, Kagamiyama, Higashi-Hiroshima 739-8526, Japan*
[14]*IHEP Protvino, State Research Center of Russian Federation, Institute for High Energy Physics, Protvino, 142281, Russia*
[15]*University of Illinois at Urbana-Champaign, Urbana, IL 61801, USA*
[16]*Iowa State University, Ames, IA 50011, USA*
[17]*Joint Institute for Nuclear Research, 141980 Dubna, Moscow Region, Russia*
[18]*KAERI, Cyclotron Application Laboratory, Seoul, Korea*
[19]*KEK, High Energy Accelerator Research Organization, Tsukuba, Ibaraki 305-0801, Japan*
[20]*KFKI Research Institute for Particle and Nuclear Physics of the Hungarian Academy*
of Sciences (MTA KFKI RMKI), H-1525 Budapest 114, POBox 49, Budapest, Hungary
[21]*Korea University, Seoul, 136-701, Korea*
[22]*Russian Research Center "Kurchatov Institute", Moscow, Russia*
[23]*Kyoto University, Kyoto 606-8502, Japan*
[24]*Laboratoire Leprince-Ringuet, Ecole Polytechnique, CNRS-IN2P3, Route de Saclay, F-91128, Palaiseau, France*
[25]*Lawrence Livermore National Laboratory, Livermore, CA 94550, USA*
[26]*Los Alamos National Laboratory, Los Alamos, NM 87545, USA*
[27]*LPC, Université Blaise Pascal, CNRS-IN2P3, Clermont-Fd, 63177 Aubiere Cedex, France*
[28]*Department of Physics, Lund University, Box 118, SE-221 00 Lund, Sweden*
[29]*Institut für Kernphysik, University of Muenster, D-48149 Muenster, Germany*
[30]*Myongji University, Yongin, Kyonggido 449-728, Korea*
[31]*Nagasaki Institute of Applied Science, Nagasaki-shi, Nagasaki 851-0193, Japan*
[32]*University of New Mexico, Albuquerque, NM 87131, USA*
[33]*New Mexico State University, Las Cruces, NM 88003, USA*
[34]*Oak Ridge National Laboratory, Oak Ridge, TN 37831, USA*
[35]*IPN-Orsay, Universite Paris Sud, CNRS-IN2P3, BP1, F-91406, Orsay, France*
[36]*PNPI, Petersburg Nuclear Physics Institute, Gatchina, Leningrad region, 188300, Russia*
[37]*RIKEN, The Institute of Physical and Chemical Research, Wako, Saitama 351-0198, Japan*
[38]*RIKEN BNL Research Center, Brookhaven National Laboratory, Upton, NY 11973-5000, USA*
[39]*Physics Department, Rikkyo University, 3-34-1 Nishi-Ikebukuro, Toshima, Tokyo 171-8501, Japan*
[40]*Saint Petersburg State Polytechnic University, St. Petersburg, Russia*
[41]*Universidade de São Paulo, Instituto de Física, Caixa Postal 66318, São Paulo CEP05315-970, Brazil*
[42]*System Electronics Laboratory, Seoul National University, Seoul, Korea*
[43]*Chemistry Department, Stony Brook University, Stony Brook, SUNY, NY 11794-3400, USA*
[44]*Department of Physics and Astronomy, Stony Brook University, SUNY, Stony Brook, NY 11794, USA*
[45]*SUBATECH (Ecole des Mines de Nantes, CNRS-IN2P3, Université de Nantes) BP 20722 - 44307, Nantes, France*
[46]*University of Tennessee, Knoxville, TN 37996, USA*
[47]*Department of Physics, Tokyo Institute of Technology, Oh-okayama, Meguro, Tokyo 152-8551, Japan*
[48]*Institute of Physics, University of Tsukuba, Tsukuba, Ibaraki 305, Japan*
[49]*Vanderbilt University, Nashville, TN 37235, USA*
[50]*Waseda University, Advanced Research Institute for Science and*
Engineering, 17 Kikui-cho, Shinjuku-ku, Tokyo 162-0044, Japan
[51]*Weizmann Institute, Rehovot 76100, Israel*
[52]*Yonsei University, IPAP, Seoul 120-749, Korea*
(Dated: February 2, 2008)

A three-dimensional (3D) correlation function obtained from mid-rapidity, low $p_{\rm T}$, pion pairs in central Au+Au collisions at $\sqrt{s_{NN}}$=200 GeV is studied. The extracted model-independent source function indicates a long range tail in the directions of the pion pair transverse momentum (out) and the beam (long). Model comparisons to these distensions indicate a proper breakup time $\tau_0 \sim 9$ fm/c and a mean proper emission duration $\Delta\tau \sim 2$ fm/c, leading to sizable emission time differences ($\langle|\Delta t_{\rm LCM}|\rangle \approx 12$ fm/c) partly due to resonance decays. They also suggest an outside-in "burning" of the emission source reminiscent of many hydrodynamical models.

Collisions between heavy nuclei at ultra-relativistic energies produce transient systems with energy densities much greater than that required to decompose bulk nuclear matter into quarks and gluons [1]. Such systems were predicted to have long lifetimes if a first order phase transition occurred during their formation or decay [2].

A number of interferometry studies [3] have been made to search for signals of long time delays in emissions from actual reaction sources [4]. For a Gaussian source function, assumed in the traditional Hanbury Brown Twiss (HBT) methodology, this would be signaled by an increase in the width R of the emission source function in the out direction of the Bertsch-Pratt coordinate system i.e $R_{out}/R_{side} >> 1$. No such result has been found by these HBT studies, and the reported Gaussian source functions are spheroidal with $R_{out} \approx R_{side}$ in the longitudinally co-moving system (LCMS) [4]. However, a recent study with a 1D source imaging technique [5, 6, 7], has observed a long non-Gaussian tail in the radial source function and attributed it to possible lifetime effects [8, 9]. This suggests that further study of the source image may give new insights into the reaction dynamics leading to source breakup.

Here, we extract and perform a detailed study of the 3D two-pion source function using the technique proposed by Danielewicz and Pratt [10, 11]. Namely, the 3D correlation function is first decomposed into a basis of Cartesian surface-spherical harmonics to extract the coefficients, also called moments, of the expansion. In turn, they are then imaged or fitted with a trial function to extract the 3D source function, which is then used to probe the emission dynamics of the two-pion source produced.

Au+Au data (at $\sqrt{s_{NN}}$=200 GeV) was recorded during 2004 with the PHENIX detector [12] at the Relativistic Heavy Ion Collider (RHIC). The collision vertex z (along the beam axis) was constrained to $|z| < 30$ cm of the nominal crossing point. Charged pions were detected in the east and west central arms of PHENIX, each of which subtends 90° in azimuth ϕ, and ± 0.35 units of pseudo-rapidity η. Tracking and momentum reconstruction were accomplished with the drift chamber and two layers of multi-wire proportional chambers with pad readout (PC1 and PC3). Particle momenta were measured with a resolution $\sigma_p/p = 0.7\% \oplus 1.0\%p$ (GeV/c).

Pion identification was achieved for $p_T \lesssim 2.0$ GeV/c and $p_T \lesssim 1$ GeV/c in the time of flight and electromagnetic calorimeter, respectively. For this analysis, mid-rapidity pion pairs were selected with $0.2 < p_T < 0.36$ GeV/c from semi-central $(0 - 20\%)$ Au+Au collisions at $\sqrt{s_{NN}}$=200 GeV, where p_T is half the pion pair transverse momentum. Track merging and splitting effects were removed by appropriate cuts on both the real and mixed pair distributions [9]. Systematic variations of these cuts were explored to obtain systematic error estimates; on average, they are well within

the statistical uncertainty. Hence, the pair cuts do not introduce any significant bias in the correlation function.

The 3D correlation function $C(\mathbf{q}) = N_{fgd}(\mathbf{q})/N_{bkg}(\mathbf{q})$ was constructed as a ratio of 3D relative momentum distribution for $\pi^+\pi^+$ and $\pi^-\pi^-$ pairs in the same event $N_{fgd}(\mathbf{q})$ to that from mixed events $N_{bkg}(\mathbf{q})$. $C(\mathbf{q})$ is normalised to unity for $50 < |\mathbf{q}| < 100$ MeV/c. Here, $\mathbf{q} = \frac{(\mathbf{p_1} - \mathbf{p_2})}{2}$ where $\mathbf{p_1}$ and $\mathbf{p_2}$ are the momentum 4-vectors in the pair center of mass system (PCMS). The Lorentz transformation of $\mathbf{q}$ from the laboratory frame to the PCMS is made by a transformation to the pair LCMS along the beam direction followed by a transformation to the PCMS along the pair transverse momentum [13].

To obtain the moments, the 3D correlation function $C(\mathbf{q})$, is expanded in a Cartesian surface-spherical harmonic basis [10, 11]

$$C(\mathbf{q}) - 1 = R(\mathbf{q}) = \sum_l \sum_{\alpha_1...\alpha_l} R^l_{\alpha_1...\alpha_l}(q) \, A^l_{\alpha_1...\alpha_l}(\Omega_{\mathbf{q}}),$$

(1)

where $l = 0, 1, 2, \ldots$, $\alpha_i = x, y$ or z, $A^l_{\alpha_1...\alpha_l}(\Omega_{\mathbf{q}})$ are Cartesian harmonic basis elements; ($\Omega_{\mathbf{q}}$ is the solid angle in $\mathbf{q}$ space); $R^l_{\alpha_1...\alpha_l}(q)$ are Cartesian correlation moments given by Eq. (2); and q is the modulus of $\mathbf{q}$.

$$R^l_{\alpha_1...\alpha_l}(q) = \frac{(2l+1)!!}{l!} \int \frac{d\Omega_{\mathbf{q}}}{4\pi} A^l_{\alpha_1...\alpha_l}(\Omega_{\mathbf{q}}) \, R(\mathbf{q}). \quad (2)$$

Here, the coordinate axes are oriented so that z (long) is parallel to the beam direction, x (out) points in the direction of the total momentum of the pair in the LCMS.

Correlation moments, for each order l, can be calculated from the measured 3D correlation function using Eq. (2). Eq. (1) is truncated at $l = 6$ and expressed in terms of independent even moments only. As expected from symmetry considerations, odd moments were found to be consistent with zero within statistical uncertainty; higher order moments were found to be negligible [14]. Up to order 6, there are 10 independent moments: R^0, R^2_{x2}, R^2_{y2}, R^4_{x4}, R^4_{y4}, R^4_{x2y2}, R^6_{x6}, R^6_{y6}, R^6_{x4y2} and R^6_{x2y4} where R^2_{x2} is shorthand for R^2_{xx} etc (the dependent moments are obtained from the independent ones [10, 11]). These independent moments were extracted as a function of q, by fitting the truncated series to the measured 3D correlation function with the moments as the parameters of the fit.

Figure 1 shows the correlation moments $R^l_{\alpha_1...\alpha_l}$ up to order $l = 6$. In panel (a), $R^0(q)$ is shown along with $R(q) = C(q) - 1$; both represent angle-averaged correlation functions, but they are obtained by very different methods. For $R^0(q)$ one uses Eq. (2) and the 3D correlation function. For $R(q)$, one simply evaluates the 1D correlation function directly as in Ref. [9].

The very good agreement between $R^0(q)$ and $R(q)$ underlines the absence of any significant angular acceptance issues and attests to the reliability of the moment extraction technique used. Figures 1(b)-(j) show results for the
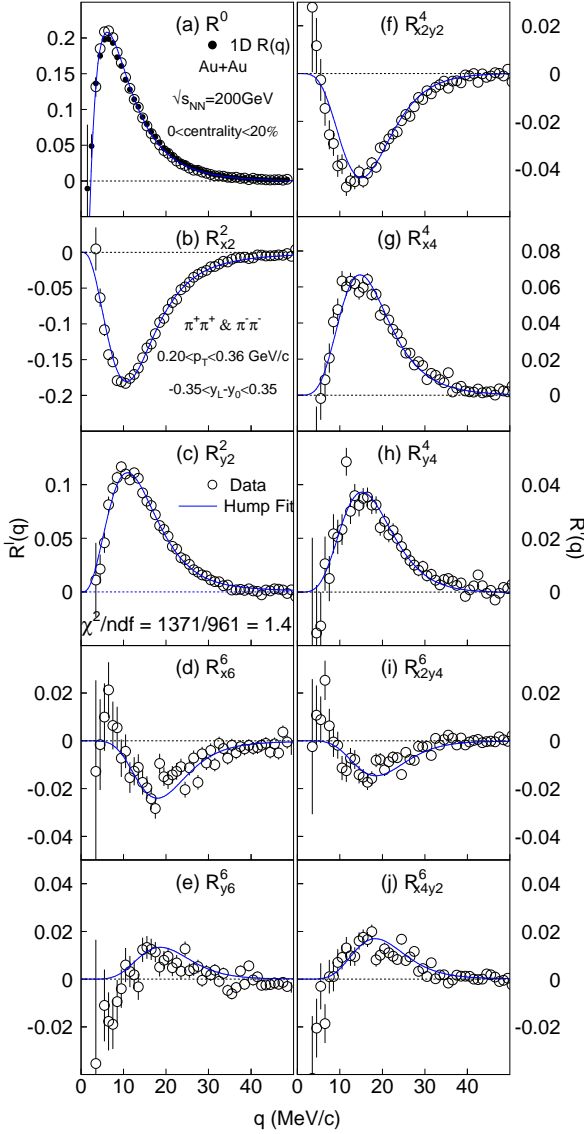
FIG. 1: Experimental correlation moments $R^l(q)$ for $l =0, 2, 4, 6$. Panel (a) also shows a comparison between $R^0(q)$ and $R(q)$. Systematic errors are less than the statistical errors. The solid lines indicate the fit with the Hump function Eq. (6).

moments $l= 2, 4$ and 6. Contributions decrease with increasing l in each direction and are relatively small for $l =6$. This justifies the truncation of the series Eq. (1) at $l =6$. The 3D source function $S(\mathbf{r})$ is obtained from these moments via imaging or fitting as discussed below.

Analogous to Eq. (1), $S(\mathbf{r})$ can be expanded in a Cartesian Surface-spherical harmonic basis (Eq. (3))

$$S(\mathbf{r}) = \sum_l \sum_{\alpha_1...\alpha_l} S^l_{\alpha_1...\alpha_l}(r) \, A^l_{\alpha_1...\alpha_l}(\Omega_{\mathbf{r}}). \quad (3)$$

Substitution of the series for $R(\mathbf{q})$ and $S(\mathbf{r})$ into the 3D Koonin-Pratt equation [3];

$$C(\mathbf{q}) - 1 = R(\mathbf{q}) = \int d\mathbf{r} K(\mathbf{q}, \mathbf{r}) S(\mathbf{r}), \quad (4)$$

gives a set of 1D relations (Eq. (5)) [10, 11]

$$R^l_{\alpha_1...\alpha_l}(q) = 4\pi \int dr r^2 K_l(q,r) S^l_{\alpha_1...\alpha_l}(r), \quad (5)$$

which connects the correlation moments $R^l_{\alpha_1...\alpha_l}(q)$ and source moments $S^l_{\alpha_1...\alpha_l}(r)$. $S(\mathbf{r})$ gives the probability of emitting a pair of particles with a separation vector $\mathbf{r}$ in the PCMS. The 3D Kernel, $K(\mathbf{q}, \mathbf{r})$, incorporates Coulomb interaction and Bose-Einstein symmetrization. Strong interaction is assumed to be negligible for pions. The 1D imaging code of Brown and Danielewicz [5, 6, 7] was used to numerically invert each correlation moment $R^l_{\alpha_1...\alpha_l}(q)$ to extract the corresponding source moment $S^l_{\alpha_1...\alpha_l}(r)$; the latter were then combined as in Eq. (3) to obtain the source function.

The 3D source function can also be extracted by directly fitting the 3D correlation function with an assumed functional form for $S(\mathbf{r})$. This corresponds to a simultaneous fit of the ten independent moments. A 4-parameter 3D Gaussian (ellipsoid) fit, using MINUIT minimization, gives a poor result (χ^2/ndf=3.7). The solid line in Fig. 1 shows the result of a fit to the independent moments with an empirical Hump function given by

$$S^H(r_x, r_y, r_z) = \lambda \exp[-f_s(\frac{x^2}{4r_{xs}^2} + \frac{y^2}{4r_{ys}^2} + \frac{z^2}{4r_{zs}^2})$$
$$-f_l(\frac{x^2}{4r_{xl}^2} + \frac{y^2}{4r_{yl}^2} + \frac{z^2}{4r_{zl}^2})], \quad (6)$$

where $\lambda, r_0, r_{xs}, r_{ys}, r_{zs}, r_{xl}, r_{yl}, r_{zl}$ are fit parameters and $f_s = 1/[1+(r/r_0)^2]$, $f_l = 1 - f_s$. This 8-parameter Hump function achieves a better fit to the data (χ^2/ndf=1.4). Smearing the track momenta by the measured resolution has a negligible effect on the data points and fits.

Figure 2(a)-(c) shows a comparison of profiles of the two-pion 3D source function in the x, y and z directions ($S(r_x)$, $S(r_y)$ and $S(r_z)$) obtained via fitting (line) and source imaging (squares). Source image extraction makes no assumption for the shape of the 3D source function; whereas, moment fitting explicitly assumes a shape. Therefore, the good agreement from the two extraction methods confirms the sufficiency of the Hump function but not its uniqueness.

The function $S(r_x)$ is characterized by a long tail, which is resolved up to ~60 fm, in contrast to $S(r_y)$ and $S(r_z)$ which range up to ~25 fm. This difference is also reflected in the respective correlation profiles (Fig. 2(d)-(f)) obtained by summation of the data (circle), fit (line) and image (square) moments up to order $l = 6$ (Coulomb effects are not removed). The broader $S(r_x)$ is associated with the narrower $C(q_x)$ (Fig. 2(a) and (d)), as expected.

The extended tail lies along the total momentum of the pair in the LCMS. Thus, the relative emission times between the pions (including those from resonances), as well as the source geometry, will contribute directly to
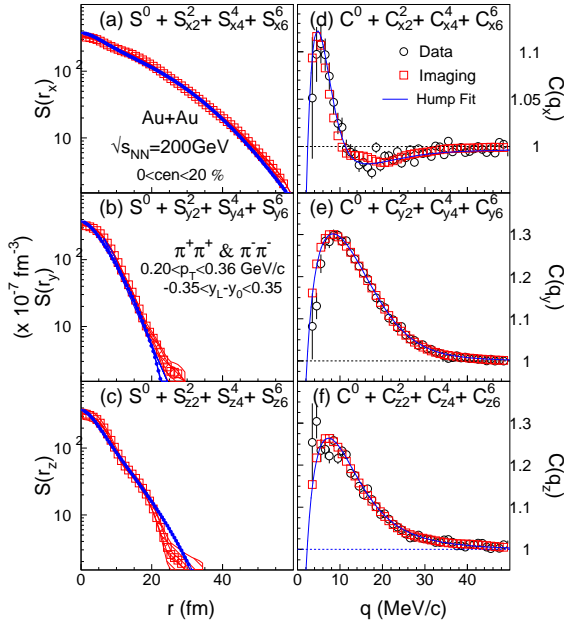
FIG. 2: Source function profiles $S(r_x)$, $S(r_y)$ and $S(r_z)$ (left panels) and their associated correlation profiles $C(q_x)$, $C(q_y)$ and $C(q_z)$ (right panels) in the PCMS. Symbols are as indicated. The bands indicate statistical and systematic errors.

FIG. 3: Source function comparison between Therminator calculation and image for (a) $S(r_x)$, (b) $S(r_y)$, (c) $S(r_z)$ in PCMS. Panel (d) compares Δt_{LCM} from Therminator events with various assumptions for $\Delta\tau$ and resonance emission.

$S(r_x)$. The lifetime of the source contributes to the range of $S(r_z)$, and $S(r_y)$ reflects its mean transverse geometric size. The difference between $S(r_x)$ and $S(r_y)$ is thus driven by the combination of the emission time difference, the freeze-out dynamics and the kinematic (Lorentz) γ boost, which is especially important in the out direction.

The event generator Therminator [14, 15] can shed more light on the source breakup and emission dynamics. It gives thermal emission from a longitudinally oriented cylinder of radius $\rho_{\max}$, includes all known resonance decays, assumes Bjorken longitudinal boost invariance and Blast-Wave transverse expansion with radial velocity v_r semi-linear in ρ [16], i.e. $v_r(\rho) = (\rho/\rho_{\max})/(\rho/\rho_{\max} + v_t)$, where $v_t = 1.41$. A differential fluid element is a ring defined by cylindrical coordinates z and ρ; it breaks up at proper time τ in its rest frame or at time t in the lab frame, where $t^2 = \tau^2 + z^2$. The freeze-out hypersurface is given by $\tau = \tau_0 + a\rho$, where τ_0 is the proper breakup time for $\rho = 0$ and a is the space-time correlation parameter. In Blast-Wave mode, Therminator sets $a = -0.5$ for source emission or "burning" from outside in as in many hydrodynamical models.

Using a set of parameters tuned to fit charged pion and kaon spectra [17], pion pairs from Therminator were obtained with the effects of all known resonance decay processes on and off. These pairs were then transformed to the PCMS, following the same set of kinematic cuts and Lorentz transformations as in the data analysis, to obtain $S(r_i)$ distributions for comparison with the data.

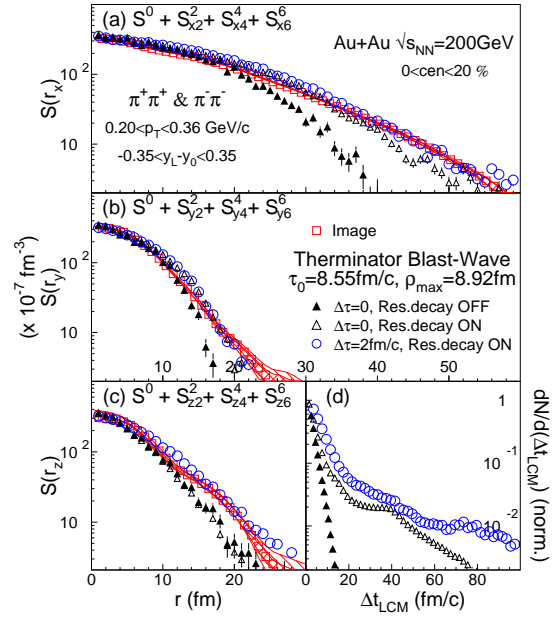Figure 3 shows that the 3D source function gener-

ated by Therminator calculations (solid triangles) with $\tau_0 = 8.55$ fm/c, $\rho_{\max} = 8.92$ fm and other previously tuned parameters [17], underestimates $S(r_x)$, $S(r_y)$ and $S(r_z)$. Open triangles (Fig. 3) show that resonance decays reproduce $S(r_y)$ ((b)) and extend the calculated source function in x ((a)) as expected, but not enough to account for the long tails in $S(r_x)$ and $S(r_z)$. This suggests that the latter have substantial contribution from pion pairs with significantly longer emission time differences. Attempts to fit the distributions by only increasing τ_0 or with $a \geq 0$ failed, suggesting a fireball burning from outside in.

The generated distribution of time differences can also be lengthened by sampling pions from a family of hypersurfaces defined by a range of values of proper breakup times τ'. One such parametrization consists of replacing τ by τ' chosen from an exponential distribution $dN/d\tau' = \frac{\Theta(\tau'-\tau)}{\Delta\tau}\exp[-(\tau'-\tau)/\Delta\tau]$. In this parametrization, the width of the distribution $\Delta\tau$ represents the mean proper emission duration in the rest frame. Figure 3 shows that this approach, with $\Delta\tau = 2$ fm/c (open circles), leads to a fairly good match to the observed source profiles in all three directions. A 10% change in $\Delta\tau$ spoils this match.

Figure 3(d) shows the relative emission time distribution in the LCMS, Δt_{LCM}, for pion pairs from events with the parameterizations indicated. For a fixed $\tau_0 = 8.55$ fm/c ($\Delta\tau = 0$) and resonance decays excluded, the distribution Δt_{LCM} is narrow, $\langle|\Delta t_{LCM}|\rangle = 2.4$ fm/c. The addition of resonance decays adds a long tail and gives $\langle|\Delta t_{LCM}|\rangle = 8.8$ fm/c. Replacing τ with the ex-

ponential distribution τ' with $\Delta\tau = 2$ fm/c, results in a Δt_{LCM} distribution which is significantly broadened to give $\langle|\Delta t_{LCM}|\rangle = 11.8$ fm/c. The wider distribution of time delays is needed to reproduce the source distributions. This implies a finite non-zero proper emission duration in the emission rest frame. Note that this Δt_{LCM} distribution broadening has only a small effect on $S(r_y)$.

Figure 3 shows that substantial time differences Δt_{LCM} are required by the source distensions; however, the interplay between proper time and breakup dynamics is model dependent. The picture which emerges from the data, in the context of the Therminator model, is consistent with that of an expanding fireball with proper breakup time $\tau_0 \sim 9$ fm/c, which hadronizes and emits particles over a short but non-zero mean proper emission duration $\Delta\tau = 2$ fm/c.

In summary, a new model-independent, three-dimensional source imaging technique has been applied to extract the 3D pion emission source function in the PCMS frame from Au+Au collisions at $\sqrt{s_{NN}} = 200$ GeV. The source function has a much greater extent in the out (x) and long (z), than in the side (y) direction. Therminator model comparison indicates a fireball burning from outside in with proper lifetime $\tau_0 \sim 9$ fm/c and a mean emission duration $\Delta\tau \sim 2$ fm/c, leading to significant relative emission times ($\langle|\Delta t_{LCM}|\rangle \approx 12$ fm/c), including those due to resonance decay.

* Deceased
† PHENIX Spokesperson: jacak@skipper.physics.sunysb.edu
[1] Nucl. Phys. **A 774** (2006).
[2] S. Pratt, Phys. Rev. Lett. 53, 1219 (1984).
[3] S. E. Koonin, Phys. Lett. **B 70**, 43 (1977).
[4] M. Lisa et al, Annu. Rev. Nucl. Part. Sci. 55, 357, (2005).
[5] D. Brown and P. Danielewicz, Phys. Lett. **B 398**, 252 (1997).
[6] D.A. Brown and P. Danielewicz, Phys. Rev. **C 57**, 2474 (1998).
[7] D.A. Brown and P. Danielewicz, Phys.Rev.**C 64**, 14902 (2001).
[8] P. Chung et al, Nucl. Phys. A 749, 275c (2005).
[9] S.S. Adler et al., Phys. Rev. Lett. **98**, 132301 (2007).
[10] P. Danielewicz and S. Pratt, Phys.Lett.**B 618** 60 (2005).
[11] P. Danielewicz and S. Pratt, nucl-th/0612076v2 (2007).
[12] K. Adcox et al, Nucl. Inst. Methods Phys. Res. Sect. **A 499**, 469 (2003).
[13] R. Lednicky et al., Phys. Part. Nucl. **35**, S50 (2004).
[14] P. Chung et al, J. Phys. G: Nucl. Part. Phys. **34** 1 (2007)
[15] A. Kisiel et al, Comput. Phys. Commun. 174, 669 (2006)
[16] A. Kisiel, Brazilian Journal Physics **37**, 3A, 917 (2007).
[17] A. Kisiel, W. Florkowski, W. Broniowski, and J. Pluta, Phys. Rev. **C 73**, 064902 (2006).; Values used are: $T = 165.6$ MeV for temperature, $\mu_B = 28.5$ MeV, $\mu_S = 6.9$ MeV, and $\mu_I = -0.9$ MeV for baryon, strangeness, and isospin chemical potentials.